Article

Multiphase Fluid Dynamics in a Vertical Pyrolysis Reactor Using Computational Fluid Dynamics

Diana Rose R. Coronado [1,2,3] and Aristotle T. Ubando [1,2,3,*]

[1] Department of Mechanical Engineering, De La Salle University, 2401 Taft Avenue, Manila 0922, Philippines
[2] Center for Engineering and Sustainable Development Research, De La Salle University, 2401 Taft Avenue, Manila 0922, Philippines
3 Thermochemical Laboratory, De La Salle University, Laguna Campus, LTI Spine Road, Laguna Blvd, Biñan 4024, Philippines
* Correspondence: aristotle.ubando@dlsu.edu.ph
Received: 10 September 2025; Revised: 29 October 2025; Accepted: 3 November 2025; Published: 13 November 2025

Abstract: This study employs Computational Fluid Dynamics (CFD) to investigate the nitrogen gas flow patterns, feedstock particle size, turbulence zones, and the distribution of the solid volume fraction in a vertical pyrolysis reactor. By employing the Eulerian multiphase model and a transient solver, the analysis allows the investigation of whether the feedstock particle size is appropriate for maintaining good mixing and identifying potential turbulence zones during the feedstock loading stage. The results highlighted the critical importance of feedstock particle size and nitrogen gas velocity in maintaining adequate mixing. Using a time-averaged profile, feedstock with a 0.55 mm diameter and a bulk density of 536 kg/m^3, combined with a continuous nitrogen gas supply at 0.485 m/s, resulted in significant bed expansion, twice the initial height. This ensures that the biomass feedstock particles do not settle at the bottom of the reactor, thus facilitating uniform heat transfer, which affects yield efficiency. The velocity of the feedstock with nitrogen gas peaked at 0.98 m/s. At 25% loading capacity, the solid-phase volume fraction decreases from 0.6 to a range of 0.1 to 0.3, indicating efficient mixing and heat transfer. It was observed that the proper nitrogen gas velocity also promotes uniform heating, enhancing the process's overall performance.

Keywords: biomass; computational fluid dynamics; fluid flow, pyrolysis; multiphase; vertical reactor

1. Introduction

The growing global energy demand and increasing carbon dioxide (CO_2) emissions due to the production of heat and power have put an urgency on implementing renewable energy sources [1]. Biomass is one of the largest renewable energy sources. It is considered carbon neutral as the amount of CO_2 released during its combustion is equal to the amount absorbed during its growth [2]. It can become carbon-negative when carbon capture, utilization, and storage (CCUS) strategies are applied [3]. During the plant's growth phase, biomass acts as a carbon sink when it sequesters atmospheric CO_2 [2]. When converted into bioenergy or other biobased materials, reliance on fossil fuels is significantly reduced, resulting in lower carbon emissions. Moreover, when processed into biochar and applied as a soil amendment, long-term carbon sequestration can be achieved by stabilizing the captured carbon instead of releasing it back into the atmosphere [4].

1.1. Pyrolysis

Pyrolysis is recognized as one of the most cost-effective technologies for converting biomass into valuable biofuels and by-products [5], namely biochar [6], bio-oil, and synthesis gas [7]. Pyrolysis is categorized into three types: slow pyrolysis, fast pyrolysis, and flash pyrolysis [8].

Slow pyrolysis is primarily used to upgrade the heating value of biomass feedstock. It uses a heating rate of 1.5 °C/s or lower, with a temperature range of 350 °C to 750 °C [9]. The parameters include the temperature, heating rate, particle size, and residence time. The product type (solid, liquid, or gas) will depend on the chosen parameters. Usually, for slow heating, feedstock heated for an extended period yielded a higher biochar yield.

Meanwhile, fast pyrolysis converts the volatiles and maximizes bio-oil production [10]. Bio-oil is obtained when the feedstock is heated at a higher temperature but for a shorter duration. This process is recommended when

a high amount of liquid product and solid biochar is unnecessary. Lastly, flash pyrolysis utilizes high temperatures and heating rates, resulting in a high bio-oil yield [8].

In addition to the different pyrolysis operating conditions, the selection and design of the reactor are also important to achieving the desired product yield and quality. Pyrolysis is typically performed using a horizontal fixed-bed reactor because of its simplicity and ease of operation [11]. However, this configuration has several drawbacks, including limited scalability, slow processing rates, and inefficient heat distribution. To address these limitations, optimizing the reactor's geometric design is crucial for achieving uniform heat transfer and consistent product yield. Therefore, fluidized bed and vertical reactor configurations were introduced, which offer improved heat and mass transfer characteristics, making them more suitable for large-scale and continuous pyrolysis applications.

1.2. Computational Fluid Dynamics

Computational fluid dynamics (CFD) is a numerical modeling approach to analyze fluid motion. It solves fluid flow by employing the Navier-Stokes equation for the fluid's mass, energy, and momentum. When using CFD, the space where fluid will flow is divided into smaller units, also known as mesh or elements. The CFD code includes a preprocessor, a flow solver, and a post-processor. The preprocessor is used for defining the problem geometry, flow parameters, grid, and boundary conditions, while the flow solver is used for the governing equations. Lastly, the post-processor is used to generate the graphical results of the simulation [12].

CFD has been employed in solving a wide range of energy-related problems, including wind energy analysis [13], building energy scenarios [14], thermal energy storage [15], turbine design [16], and even greenhouse heating [17]. Sumner, Watters and Masson [13] provided a review about using CFD to predict a wind turbine's rotor and airfoil performance under varying environmental conditions and scale models. Mohamed, Ali and Hafiz [16] used it to study a low-speed wind turbine to improve its overall performance. Tian, Han, Zuo and Sohn [14] provided a review of CFD applied to simulating the building's energy under an indoor environment. Al-abidi, Bin Mat, Sopian, Sulaiman and Mohammed [15] provided a review paper on using CFD in latent heat energy storage. Furthermore, CFD has recently been utilized to investigate thermochemical processes, including combustion, pyrolysis, and gasification [18]. The following studies explore the application of CFD in analyzing pyrolysis conditions.

Tobo*,* et al. [19] used CFD to predict biomass feedstock's flow pattern, heat flux, temperature, emissions, and ash deposits. Hartge*,* et al. [20] used a circular fluidized bed with a two-fluid model approach for the analysis. The simulation is based on a pilot-scale rectangular riser, and the study aims to determine a suitable formulation for the solid-gas flow inside the reactor. A combination of turbulence models, granular temperature, solid phase turbulence, solid-solid restitution coefficient, and drag correlations is simulated.

Kaczor*,* et al. [21] comprehensively reviewed different CFD modeling approaches for biomass pyrolysis. The paper highlights that mass and heat transport inside the reactor is crucial to the simulation. It includes the changes in the feedstock's physical properties since the pellets are simultaneously subjected to pyrolysis. However, the conversion of pellets inside the reactor varies since the pellets' distance from the heat sources varies. Therefore, the reactor's geometry should be accurately modeled to capture thermal conditions. Meanwhile, the review paper summarizes CFD's recent application for biomass's multi-scale pyrolysis set-up. These include using CFD to understand mass and heat transfer using microwave-assisted pyrolysis and solar-assisted reactors.

Investigating the behavior of different feedstocks in a biomass reactor using CFD was also reported in the literature. Janajreh and Raza [22] utilized CFD to study the flow patterns of waste tires using gasification technology. Their research employed a two-stage conversion process, combining proximate and ultimate analysis with Gibbs energy minimization. Khodaei, Álvarez-Bermúdez, Chapela, Olson, MacKenzie, Gómez and Porteiro [7] utilized the Eulerian framework within commercially available CFD software to model the thermochemical processing of waste wood chips sourced from construction and demolition activities. Their study aimed to optimize various aspects of biochar production, focusing on parameters such as biochar yield, heat transfer mechanisms across multiple zones, wood chip shrinkage, tar and volatile composition, and overall energy efficiency. The researchers specifically investigated the thermochemical conversion processes occurring within a bed reactor. A significant emphasis was placed on understanding how heat transfer and chemical reactions are influenced by the spatial separation of different reaction zones, particularly the drying and pyrolysis stages. The study revealed that decoupling these processes could result in substantial energy savings and quality improvements. According to the CFD analysis, isolating the drying zone from the pyrolysis zone could reduce energy consumption during the drying phase by at least 31%. This separation minimizes unnecessary heat loss and enhances thermal efficiency, resulting in a more sustainable operation. Furthermore, the biochar quality produced through this approach showed a notable enhancement, with a 21% increase in carbon content.

Pourhoseinian*,* et al. [23] conducted a comparative study on the fast pyrolysis of hardwood (red oak), herbaceous biomass (switchgrass), and softwood (Picea glauca) using CFD. The research aimed to analyze the

influence of feedstock type and critical parameters, including density, volume fraction, and temperature distribution, bio-oil yield, and other pyrolysis products. The numerical simulations showed high accuracy, with an acceptable error margin of less than 13% compared to experimental results. This validation underscores the reliability of CFD in modelling complex thermochemical processes. The study revealed significant differences in bio-oil yields based on the type of feedstock. Among the three materials, hardwood produced the highest yield, followed by herbaceous biomass, while softwood generated the least amount of bio-oil. The study also examined the impact of varying operating conditions, specifically temperature and particle size, on pyrolysis outcomes. The simulations identified optimal conditions for maximizing bio-oil production at a temperature of 500 °C and a particle size of 400 μm. At this temperature, the thermochemical reactions efficiently converted the feedstock into volatile products, minimizing the formation of gas and char. The simulation results also demonstrated that increasing the temperature beyond the optimal range led to a higher gas yield at the expense of bio-oil production. Conversely, increasing particle size promoted higher char production due to reduced heat transfer efficiency and slower reaction rates. These findings offer valuable insights for optimizing pyrolysis processes to achieve the desired product distribution. This study highlights the versatility and accuracy of CFD as a predictive tool for biomass conversion processes. By enabling the detailed analysis of feedstock characteristics and operating conditions, CFD can support the development of efficient and sustainable bio-oil production methods tailored to specific types of biomass. The findings contribute to advancing bioenergy technologies and optimizing resource utilization in the context of renewable energy solutions.

Wang, et al. [24] employed CFD to investigate the municipal solid waste (MSW) pyrolysis process using high-temperature flue gases as the heat source. The study analyzed four key components of MSW to assess the effects of flue gas properties on reaction characteristics and heat transfer dynamics during the pyrolysis process. The numerical simulations provided valuable insights into the influence of flue gas temperature, velocity, and mixing methods on the behavior of feedstock and system performance. One of the primary findings was that increasing the flue gas velocity resulted in higher flue gas consumption, thereby reducing the overall energy efficiency of the pyrolysis process. This result highlights the importance of optimizing flue gas flow rates to strike a balance between effective heat transfer and energy conservation. Temperature also played a crucial role in determining pyrolysis efficiency. The study revealed that raising the flue gas temperature from 973 K to 1273 K significantly reduced the pyrolysis time by 34.37%. This reduction highlights the potential for high-temperature flue gases to accelerate the thermal decomposition of waste materials, leading to faster conversion of feedstock into valuable products such as biochar, syngas, and bio-oil. However, higher temperatures may require careful energy management to prevent inefficiencies elsewhere in the system. The research further demonstrated how mixing methods impacted the uniformity of heat distribution across the feedstock. Adequate mixing improved the consistency of the pyrolysis reaction, reducing localized overheating or under-processing of the waste materials.

CFD also has emerged as a valuable tool for investigating the kinetics and reactivity of biomass during pyrolysis. This technique enables the detailed analysis of both primary and secondary reaction mechanisms, as well as the associated physical phenomena, such as particle shrinkage and internal convection within the reactor. Kamila, et al. [25] conducted a study using a 2-dimensional CFD model to examine the pyrolysis of large wood. The study focused on the behavior of biomass particles during pyrolysis, considering factors like pressure distribution, velocity, mass fraction, and temperature variations within the feedstock. The results indicated that these factors significantly influence the overall pyrolysis process, including the reaction rate and product yield. Sangaré, Moscosa-Santillan, Bostyn, Belandria, De La Cruz Martínez and Van De Steene [9] investigated the kinetics of lignocellulosic biomass undergoing slow pyrolysis. Their model incorporated a multi-step kinetic scheme, integrating mass transfer, momentum, and heat transfer to capture the complex interactions occurring during pyrolysis. The simulation results were validated against experimental data, demonstrating the model's accuracy. For example, the predicted yield of non-condensable gases showed an average relative error of 11.59% for avocado biomass and 6.90% for cellulose. Regarding biochar yield, the errors were 9.74% for cellulose and 6.41% for avocado. These findings underscore the reliability of CFD simulations in predicting product yields with reasonable accuracy, highlighting the potential for optimizing pyrolysis processes for different biomass types. Wang, et al. [26] took a multiscale approach to model biomass pyrolysis by incorporating the Discrete Element Method (DEM) within a CFD framework. This method provides a more detailed representation of intraparticle kinetics, reactor dynamics, and the interactions between biomass particles during pyrolysis. The study emphasized the importance of considering both the micro-scale (particle level) and macro-scale (reactor level) factors to better understand the overall pyrolysis process and improve reactor design. These studies demonstrate the increasing potential of CFD models in enhancing our understanding of biomass pyrolysis. By simulating the complex interactions of thermal, chemical, and physical processes, CFD enables more efficient biomass conversion technologies, which are crucial for developing sustainable bioenergy solutions.

From the literature review, maintaining an inert condition is necessary to ensure that there will be minimal oxidation and a good conversion process [27]. Factors such as feedstock particle size and the loading rate within the reactor should be monitored to enhance interactions between the solid and gas phases [23]. The application of CFD to pyrolysis studies is summarized in Table 1.

Table 1. Computational fluid dynamics applied to pyrolysis.

Investigated Parameters	References
Flue gas velocity	Wang, Jia, Song, Yin, Chen and Qian [24]
Shrinkage and internal convection	Kamila, Sadhukhan and Gupta [25]
Solid and bio-oil yield	Sangaré, Moscosa-Santillan, Bostyn, Belandria, De La Cruz Martínez and Van De Steene [9]
Bio-oil yield	Pourhoseinian, Asasian-Kolur and Sharifian [23]
Multizone heat transfer concepts,	Khodaei, Álvarez-Bermúdez, Chapela, Olson, MacKenzie, Gómez and Porteiro [7]
Flow pattern, heat flux, temperature, emissions, and ash deposits	Tobo, Lotfi, Virla and Mahinpey [19]
Flow patterns in gasification process	Janajreh and Raza [22]
Suitable formulation for the solid-gas flow inside the reactor	Hartge, Ratschow, Wischnewski and Werther [20]
Feedstock particle size, inert gas velocity, and mixing flow behavior	This study

1.3. Scope and Novelty of the Study

This study presents a novel investigation into the fluid flow dynamics, particle behavior, and mixing conditions within a biomass pyrolysis reactor, under both loaded and unloaded scenarios, using the Eulerian multiphase model. An even distribution of biomass particles within the reactor indicates good fluidization and adequate mixing, which are essential for uniform heat transfer and efficient reaction progression. In contrast, regions of high biomass concentration may indicate agglomeration or inadequate gas penetration, while low solid volume fractions in the upper regions could signify bed expansion. These findings provide insight into the effectiveness of inert nitrogen gas dispersion and the spatial distribution of the feedstock, key parameters that influence pyrolysis performance.

No prior study has systematically examined the mixing behavior between feedstock particles and nitrogen gas within the reactor during the early pyrolysis phase. This research addresses that gap by analyzing the interaction between feedstock particle size and inert gas dynamics. The analysis of solid volume fraction distributions provides meaningful insights into feedstock movement and fluidization quality, offering a valuable basis for improving process efficiency, thermal uniformity, and product yield.

2. Materials and Methods

This section details the materials and methodology employed to simulate and analyze the flow dynamics within a vertical reactor. The vertical reactor dimension was modeled using SolidWorks 2024, while the flow analysis was performed using ANSYS 2024, a commercially available computational software. The study was conducted with the following specifications: a 20-core processor, 1 TB SSD storage, 32 GB memory, and an 8 GB GDDR6 video card.

2.1. Dimension and Operating Conditions of the Reactor

The reactor's dimensions used in this study were adopted from the model Makkawi and Mohamed [28]. It is a two-dimensional model with a reactor length of 36 cm and a width of 8 cm, as shown in Figure 1a. To provide an inert condition, nitrogen gas was introduced at the bottom of the reactor at a constant velocity of 0.485 m/s. Before adding the feedstock, the reactor was preheated to a temperature of 800 K. A no-slip condition was assumed for the wall boundary condition, indicating that there was no significant motion between the wall surface and the fluid. The studies mentioned previously also supported the wall boundary condition [23]. The initial condition for the multiphase analysis is presented in Table 2.

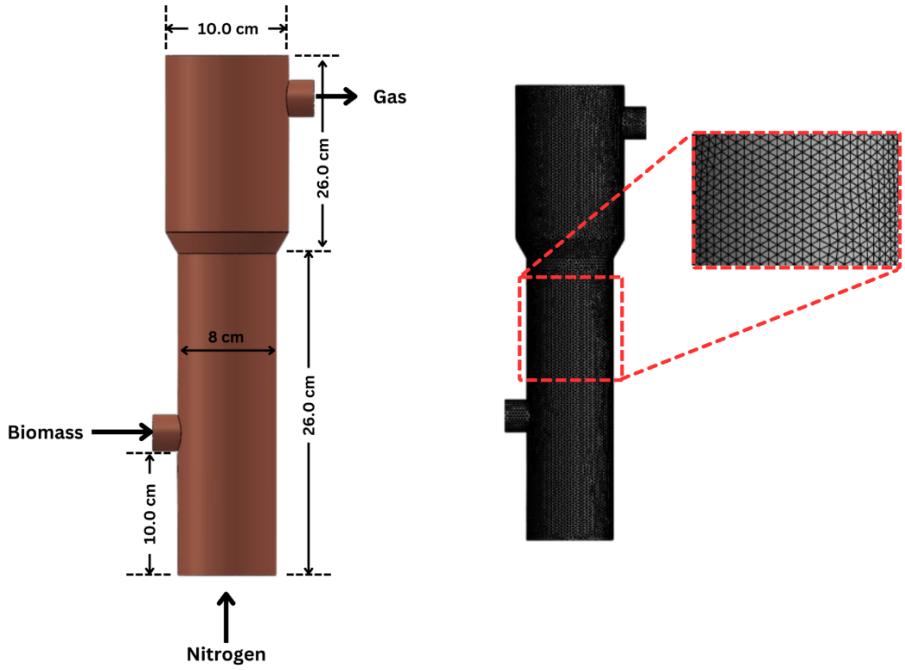

(**a**) (**b**)

Figure 1. Vertical reactor (**a**) Computer-Aided Design Model (**b**) Discretization Model.

Table 2. Initial condition for the multi-phase analysis [28].

Phase	Species	Diameter (mm)	Temperature (K)	Mass Faction	Volume Fraction	Superficial Velocity (m/s)
Primary Phase	Nitrogen Gas	-	800	1	0.40, 1	0.485
Secondary Phase	Feedstock	0.55	300	1	0.60, 0	-

The feedstock, adopted from the study of Makkawi and Mohamed [28], with a particle size of 0.5 mm, a density of 536 kg/m^3, and a temperature of 300 K, was then introduced into the reactor through the lateral side. The solid volume fraction used was 0.60, with a maximum limit of 0.63. This is similar to the maximum limit used by Pourhoseinian, Asasian-Kolur and Sharifian [23]. The species' physical properties are shown in Table 3.

Table 3. Species physical properties [28].

Species	Density (kg/m^3)	Diameter (mm)	Temperature (K)	Molecular Weight (g/mol)	Heat Capacity (J/kg K)	Thermal Conductivity
Feedstock	536	0.55	300	165	2300	0.3
Nitrogen Gas	-	-	800	28	1121	5.63×10^{-2}

2.2. Mesh Independence and Convergence Criteria

Mesh independence and convergence criteria were also considered in the study to validate the robustness and accuracy of the results. These measures ensure that the results were not dependent on the element size or number of cells. This was achieved by reducing the mesh into smaller elements until the results became stable, indicating that further refinement had negligible effects on the outcomes.

Convergence criteria were also applied to ensure the robustness of the simulation. The simulation was conducted in transient mode to accurately capture the system's time-dependent behavior. A total of 1000-time steps was defined, each with a time step size of 0.001 s, and up to 10 iterations were performed per time step. At every time step, residuals were monitored to ensure convergence, with threshold values set to 1×10^{-3} for continuity, 1×10^{-4} for the momentum and turbulence, and 1×10^{-6} for the energy equation. These criteria ensured numerical stability and solution accuracy throughout the simulation.

2.3. Model Description and Governing Equation

Multiphase flow simulation utilizes various computational models to analyze phase interactions between fluids. Among these, the Eulerian multi-fluid model is a widely used approach. The Eulerian multi-fluid model is discussed in the following subsection, including its governing equations and typical applications.

2.3.1. Eulerian Multi-Fluid Model

The Eulerian Multi-Fluid Model was used to simulate the solid and gas phases of the pyrolysis reactor. The nitrogen gas is the primary gas phase, while the biomass feedstock is the secondary solid phase. The solution follows the methodology of Pourhoseinian, Asasian-Kolur and Sharifian [23]. The finite volume method was employed for the domain, a first-order upwind scheme was used for the momentum equations, and the K-turbulence model was applied for the turbulent flow. The least square cell-based and first-order implicit methods were used for the gradient and transient calculations, respectively. A detailed summary is shown in Table 4.

Table 4. The multi-phase models.

Model		**References**
Multiphase Model	Eulerian	Makkawi and Mohamed [28]
Momentum Equation	First Order Upwind	Makkawi and Mohamed [28]
Volume Fraction	QUICK	Pourhoseinian, Asasian-Kolur and Sharifian [23]
Turbulence	k-ε Turbulence Model	Pourhoseinian, Asasian-Kolur and Sharifian [23]
Solver	Transient	
Granular Viscosity	Gidaspow et al.	Gidaspow, et al. [29]
Granular Bulk Viscosity	Lun et al.	Lun, et al. [30]
Solid Pressure	Syamlal-obrien	Syamlal [31]
Packing Limit	0.63	Makkawi and Mohamed [28] Pourhoseinian, Asasian-Kolur and Sharifian [23]
Radial Distribution	Lun et al.	Lun, Savage, Jeffrey and Chepurniy [30]
Phase Interaction		
Gas-Solid Heat Transfer Coefficient	Gunn	Gunn [32]
Restitution Coefficient	0.9	Makkawi and Mohamed [28]
Gravity	9.81 m/s	-

2.3.2. Governing Equations

The mathematical model is a set of governing equations that describe the behavior of both solid and gas phases, as summarized in Table 5. These include equations for continuity, energy, momentum, and granular temperature.

Table 5. The governing equations used in this study [28].

Phase	**Equation**
Continuity equation	
Gas phase	$\frac{\partial}{\partial t}\left(\alpha_g \rho_g\right) + \nabla \cdot \left(\alpha_g \rho_g \vec{V}_g\right) = S_g$
Solid Phase	$\frac{\partial}{\partial t}\left(\alpha_{sn} \rho_{sn}\right) + \nabla \cdot \left(\alpha_{sn} \rho_{sn} \vec{V}_{sn}\right) = S_{sn}$
Momentum equation	
Gas phase	$\frac{\partial}{\partial t}\left(\alpha_g \rho_g \vec{V}_g\right) + \nabla \cdot \left(\alpha_g \rho_g \vec{V}_g \vec{V}_g\right) = -\alpha_g \nabla p + \nabla \cdot \bar{\bar{\tau}}_g + \alpha_g \rho_g \vec{g} + \sum_{n=1}^{2} \beta_n \left(\vec{V}_{sn} - \vec{V}_g\right) + S_g^v$
Solid Phase	$\frac{\partial}{\partial t}\left(\alpha_{sn} \rho_{sn} \vec{V}_{sn}\right) + \nabla \cdot \left(\alpha_{sn} \rho_{sn} \vec{V}_{sn} \vec{V}_{sn}\right) = -\alpha_{sn} \nabla p + \nabla \cdot \overline{\overline{\tau_{sn}}} + \alpha_{sn} \rho_{sn} \vec{g} + \beta_n \left(\vec{V}_g - \vec{V}_{sn}\right) + \zeta_{nm} \left(\vec{V}_{sn} - \vec{V}_{sn}\right) + S_{sn}^v$
Energy Equation	
Gas phase	$\frac{\partial}{\partial t}\left(\alpha_g \rho_g H_g\right) + \nabla \cdot \left(\alpha_g \rho_g \vec{V}_g H_g\right) = \nabla \cdot \left(K_g \nabla T_g\right) + \sum_n \left[h_{gsn}\left(T_{sn} - T_g\right)\right] + S_g^H$

Table 5. *Cont.*

Phase	Equation
Energy Equation	
Solid Phase	$\frac{\partial}{\partial t}\left(\alpha_{sn}\rho_{sn}H_{sn}\right)+\nabla\cdot\left(\alpha_{sn}\rho_{sn}\vec{V}_{sn}H_{sn}\right)=\nabla\cdot\left(K_{sn}\nabla T_{sn}\right)+h_{gsn}\left(T_g-T_{sn}\right)+S_{sn}^{H}$
Granular Temperature Equation	
Solid Phase	$\frac{3}{2}\left[\frac{\partial}{\partial t}\left(\alpha_{sn}\rho_{sn}\Theta_{sn}\right)+\nabla\cdot\left(\alpha_{sn}\rho_{sn}\vec{V}_{sn}\Theta_{sn}\right)\right]=\overline{\overline{\tau_{sn}}}:\nabla\vec{V}_{sn}+\nabla\cdot\left(k\Theta_{sn}\nabla\Theta_{sn}\right)$ $-\gamma\Theta_{sn}-3(\beta_n+\zeta_{nm})\Theta_{sn}$

2.4. Flow Investigation Using the Eulerian Multiphase Model

Different behaviors inside the reactor were investigated in this study. This includes the flow pattern, velocity distribution, turbulence zone inside the reactor, with and without load, and solid volume fraction. These assessments will provide a baseline understanding of the reactor's fluid dynamics and insight into its design implications.

2.4.1. Nitrogen Gas Flow in an Empty Reactor

The behavior of nitrogen gas as it flows through the reactor in its empty state serves as the baseline model. This establishes how the reactor's design affects fluid flow, including velocity gradients and turbulence generation. The baseline assessment is also critical for comparing scenarios where the reactor operates under load conditions. Adding materials or feedstock is expected to significantly alter the flow patterns, creating zones of increased turbulence or restricted flow. By first understanding the fluid behavior in the empty reactor, the study can better assess how these changes affect the overall process when a load is introduced. For the analysis, a nitrogen gas flow rate of 0.485 m/s and a temperature of 800 K were used.

2.4.2. Biomass Feedstock Loading Rate

The feedstock at a mass flow rate of 0.1 kg/s and temperature of 300 K, along with nitrogen gas at 800 K, was introduced at the lateral side, with a continuous flow of nitrogen gas at the bottom. This facilitates a controlled atmosphere and a stable inert environment needed during the thermochemical conversion. The interaction between the gas and solid phases was simulated to identify the behavior of the feedstock during the loading stage. This analysis is crucial for identifying potential issues, such as flow disruptions or uneven material distribution, that may arise during this stage.

2.4.3. Biomass Feedstock and Nitrogen Gas Mixing Behavior

Efficient mixing of the solid feedstock and nitrogen gas is crucial for achieving a uniform temperature distribution and enhancing heat transfer efficiency within the reactor. Since the activation energy of biomass pyrolysis directly influences the thermal decomposition rate, maintaining controlled and homogeneous reaction conditions is essential. The activation energy of biomass pyrolysis governs the rate of biomass thermal decomposition. Date palm biomass activation energy ranges from 49.8×10^3 J/mol to 89.1×10^3 J/mol [33]. For volatile products, thermal decomposition results in pyrolysis vapor, which consists of both condensable and non-condensable components. The condensable components, referred to as bio-oil, include hydrocarbon and water, while CO, CO_2, H_2, and CH_4 are the non-condensable gases or biogas [28]. In this study, the investigation focuses on the flow dynamics, specifically examining the interaction between nitrogen gas and feedstock within the reactor. The biomass feedstock was set at 25% capacity, occupying a height of 9.5 cm from the bottom of the reactor. Nitrogen gas was introduced at the bottom at a velocity of 0.485 m/s, while at the lateral side, where the feedstock was initially fed, at a velocity of 0.1 m/s.

Lastly, solid volume fraction indicates the concentration of solid material in the multiphase system. The value of 0 indicates that no solid particles are present in the controlled volume, while 100% indicates that the entire volume is filled with solid. In this study, a solid volume fraction of 60% was used, as adopted from the study of Makkawi and Mohamed [28].

3. Results and Discussions

The following section presents the results of the mesh independence test and convergence analysis, followed by the multiphase analysis, involving the feedstock particle, feedstock loading rate, and nitrogen gas velocity.

3.1. Mesh Independence and Convergence Criteria

A mesh independence study was conducted to ensure that the results obtained are accurate and not dependent on the mesh size. The continuity residual was monitored during each iteration as part of the convergence criteria. Convergence was assessed based on the residuals of the governing equations, which indicate the accuracy and stability of the numerical solution. For the multiphase analysis, a residual threshold of 1×10^{-3} was obtained for the momentum and continuity equations, and 1×10^{-6} for the energy equation.

Model 1, with a 0.01 mesh, 0.01 element size, and 439 nodes, achieved a continuity of 10^{-3}, indicating that the solution had already converged. The time step size was 0.001 s, with 100-time steps and 10 iterations per time step. Changing the mesh to Model 2, with an element size of 0.005, resulted in a convergence of 10^{-4}, achieved with 37,621 elements and 38,167 nodes. The time step size is 0.001 s, with an increased number of time steps to 1000 and 10 iterations per time step. Lastly, Model 3 is reduced to 0.0005 mesh, comprising 150,497 elements and 151,591 nodes, achieving a convergence result of 10^{-7}. The number of time steps, time step size, and iterations were similar to Model 2. A detailed summary of mesh independence is tabulated in Table 6. The graphical illustration of the mesh is shown in Figure 1b.

Table 6. Parameters for mesh independence.

Criteria	1	2	3
Size	0.0100	0.0050	0.0005
Element	381	37,621	150,497
Node	436	38,167	151,591
Skewness	0.9000	0.9000	0.9000
Orthogonal	Min: 0.8562 Max: 0.9840	Min: 0.7281 Max: 0.9698	Min: 0.7067 Max: 0.9674
Time step size (s)	0.001	0.001	0.00005
Number of Time steps	100	1000	1000
Max Iterations/Time Steps	10	10	10
Continuity/ Convergence Result	10^{-3}	10^{-4}	10^{-7}

3.2. Multi-Phase Model

This chapter discusses the fluid flow behavior of nitrogen gas in an empty reactor, the introduction of feedstock with a continuous supply of nitrogen gas, and the mixing behavior of nitrogen gas and feedstock inside the biomass reactor.

3.2.1. Primary Gas Phase—Nitrogen Gas Flow in an Empty Reactor

The time-average profile of the velocity of nitrogen gas, supplied at the bottom of an empty reactor, is shown in Figure 2. To determine the flow behavior of nitrogen gas, the feedstock entry was assumed to be closed, and only the bottom of the reactor was open to supply nitrogen gas at a velocity of 0.485 m/s and a temperature of 800 K. As observed, the color pattern was consistent throughout the lower wall of the empty reactor (Figures 2a–4d), indicating that it was filled with nitrogen gas and that the inert condition necessary for the process was achieved. At the top wall of the reactor, where pyrolysis vapor exits, a minimal drop in nitrogen velocity along the edges was observed at time steps of 600 s (Figure 2e) and 800 s (Figure 2f). However, the pattern was acceptable since the feedstock will only be loaded at the lower wall. At the outlet, the velocity increased, ranging from 2.0 m/s to 2.6 m/s.

3.2.2. Secondary Solid Phase—Feedstock Loading

The feedstock was introduced from the lateral side at 0.1 kg per second, with an initial temperature of 500 K, along with nitrogen gas at 800 K. Concurrently, nitrogen gas was continuously supplied from the bottom at a velocity of 0.485 m/s and a temperature of 800 K. The time average profile of feedstock loading at various time steps is presented in Figure 3.

As shown in Figure 3a, the feedstock and nitrogen gas enter with an initial velocity of 0.0105 m/s. The velocity increases to 0.3860 m/s at 100 s (Figure 3b) and reaches 0.5330 m/s at 200 s (Figure 3c). Upon doubling the time step to 400 s (Figures 3d and 3e), the feedstock velocity accelerates to 1.04 m/s and remains consistent up to 800 s (Figure 3f).

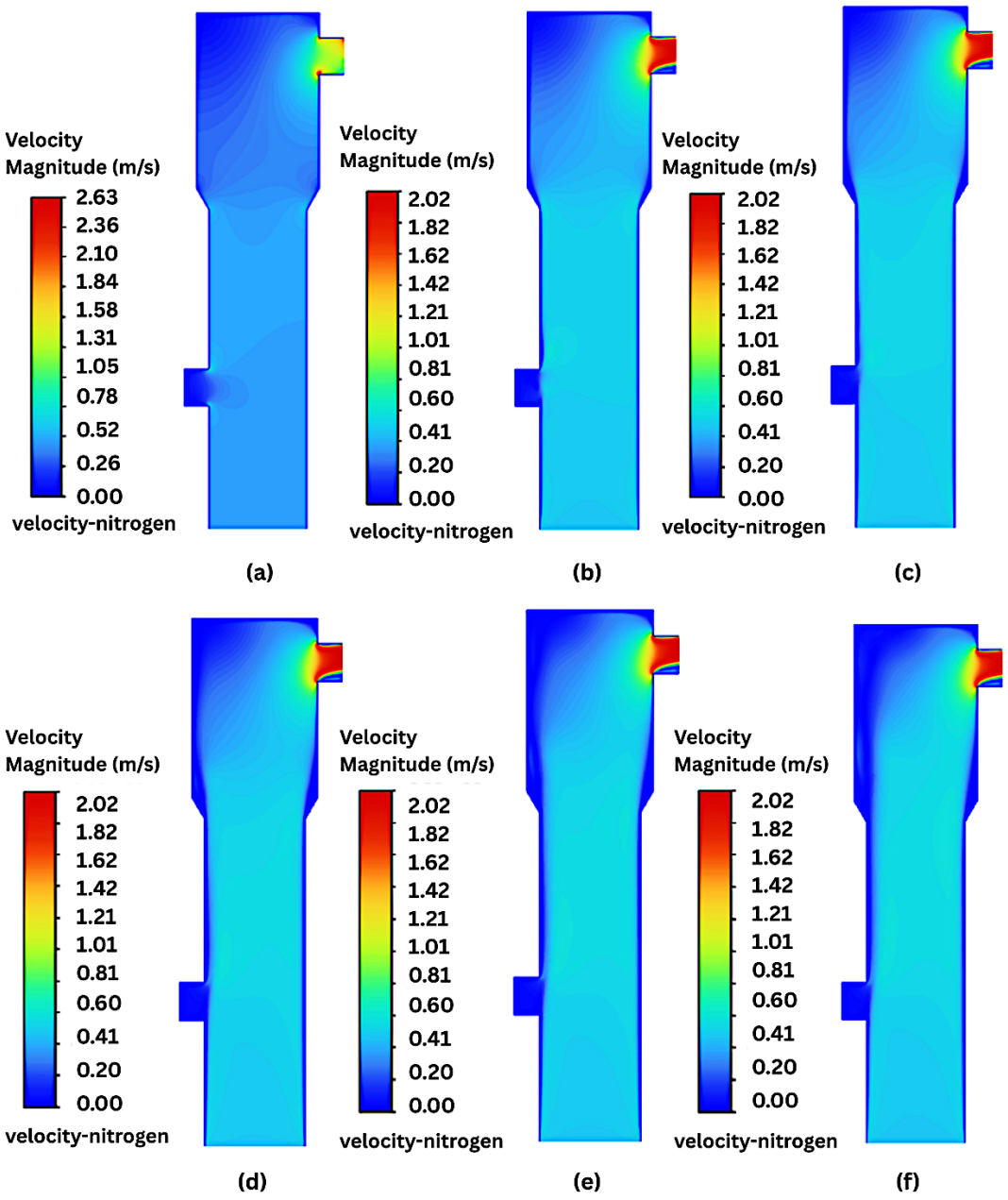

Figure 2. Time-average profile of the nitrogen gas in an empty reactor at (**a**) 0 s, (**b**) 100 s, (**c**) 200 s, (**d**) 400 s, (**e**) 600 s, (**f**) 800 s.

Meanwhile, Figure 4 presents the time-average profile of the nitrogen gas during the feedstock loading stage. Initially, the reactor was filled with nitrogen gas, as illustrated in Figure 4a,b, similar to Figure 3. At 400 s, a variation in the contour map was already observed in Figure 4c to 4d, indicating that the feedstock had already entered the lower wall of the reactor. Since the feedstock was introduced on the left side of the reactor, the velocity magnitude of the nitrogen gas increased on the right side of the reactor, as shown in Figure 4e,f.

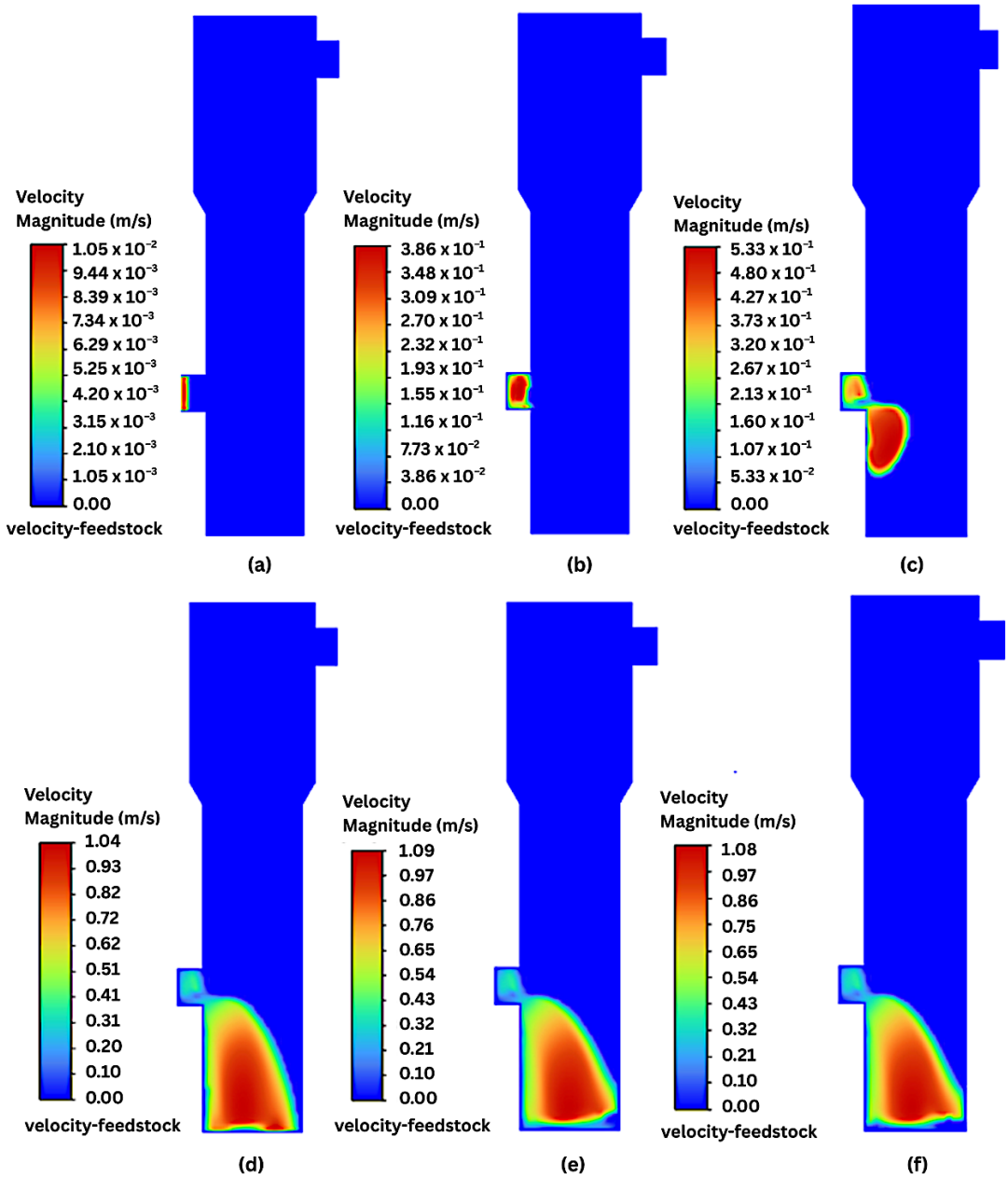

Figure 3. Time-average profile of the feedstock loading at (**a**) 0 s, (**b**) 100 s, (**c**) 200 s, (**d**) 400 s, (**e**) 600 s, (**f**) 800 s.

3.3. Primary Gas and Secondary Solid Phase Mixing Behavior

The interaction between the primary gas and secondary solid phases in a vertical reactor is crucial for optimizing product efficiency. The following subsections present a detailed analysis of the results.

3.3.1. Velocity Magnitude of the Solid Phase

The secondary solid phase, introduced into the reactor as biomass feedstock, was maintained at a fixed loading of 25%, which translates to an equivalent height of 9.5 cm from the bottom of the reactor, with nitrogen gas continuously supplied at the bottom of the reactor at 0.485 m/s and through the lateral side at 0.1 m/s. The number of time steps and time step size at 1000 and 0.001, respectively, achieved the target convergence result. The time-averaged profiles of the feedstock and nitrogen gas velocities are presented in Figures 5 and 6, respectively.

In Figure 5a, the feedstock had already been loaded into the reactor. At 100 s, reflected in Figure 5b, a change in contour was already observed. The velocity of the feedstock increases continuously (Figure 5c), indicating that the feedstock is continuously moving inside the reactor during pyrolysis, where the reactor is heated to 800 K. In

Figure 5d,e, the feedstock continued to move inside the reactor and partially reached the upper wall. This indicated that pyrolysis vapor had already started to develop.

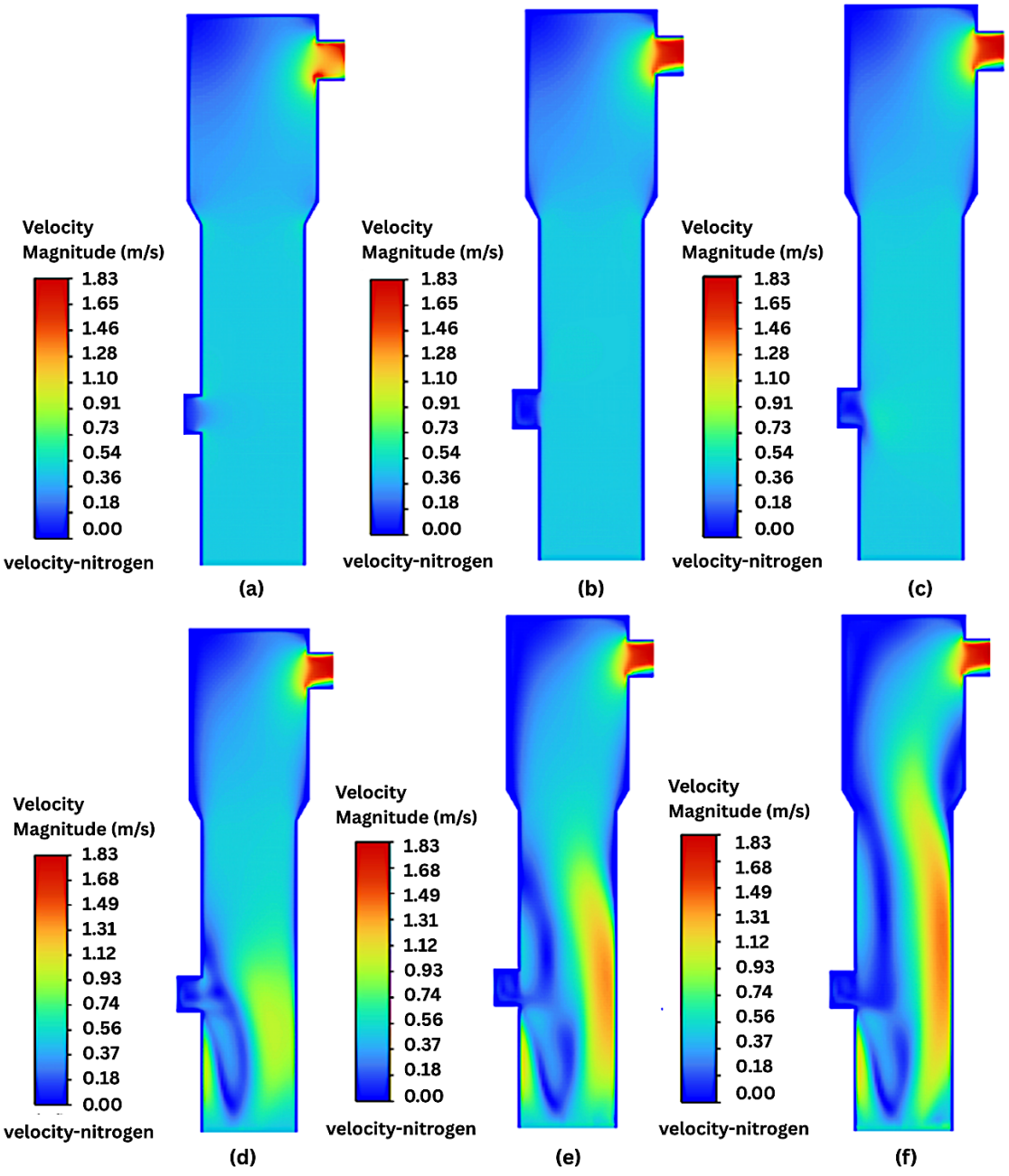

Figure 4. Time-average profile of the fluidizing nitrogen gas during the introduction of feedstock at the lateral side at (**a**) 0 s, (**b**) 100 s, (**c**) 200 s, (**d**) 400 s, (**e**) 600 s, (**f**) 800 s.

The time-averaged profile of nitrogen gas movement during the pyrolysis process is shown in Figure 6. Since the feedstock was already inside the reactor, the movement of nitrogen gas differed during the simulation of an empty reactor and at feedstock loading, as shown in Figures 2 and 4, respectively. The movement of nitrogen gas during pyrolysis was faster, reaching 3.68 m/s at a timestep of 800 s, as shown in Figure 6f.

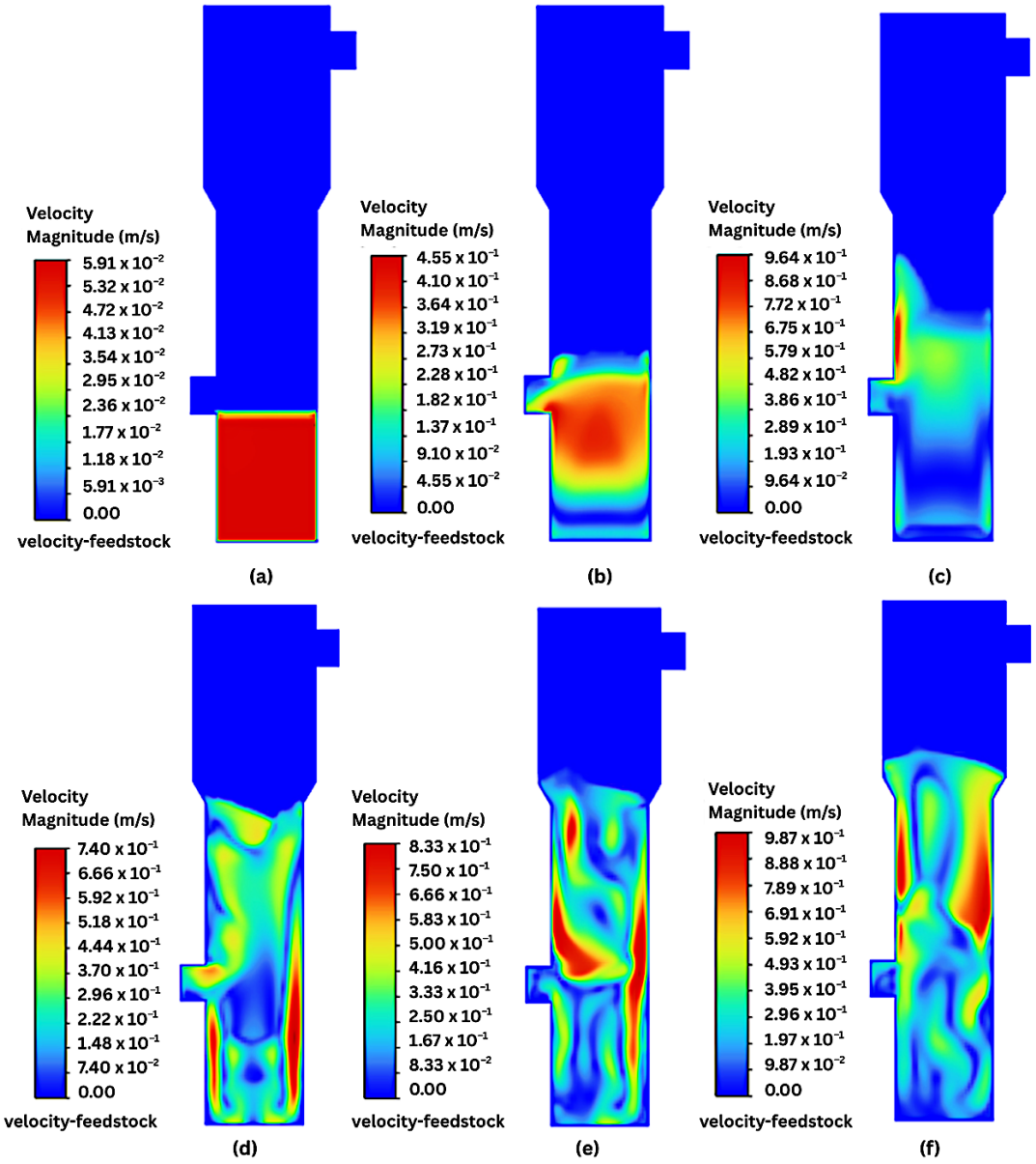

Figure 5. Time-average profile of feedstock velocity during pyrolysis at (**a**) 0 s, (**b**) 100 s, (**c**) 200 s, (**d**) 400 s, (**e**) 600 s, (**f**) 800 s.

3.3.2. Solid Volume Fractions

The volume fraction (vf) of feedstock and nitrogen gas behavior from the beginning to 200 s is shown in Figure 7a–e, respectively. At the beginning of the simulation, feedstock was loaded to 25% capacity (Figure 7a), corresponding to a 9.5 cm elevation from the reactor's bottom. In parallel, as shown in Figure 7d, nitrogen gas occupies the upper region of the reactor. At 100 s, nitrogen gas enters the bed region (Figure 7e), while the feedstock starts expanding and dispersing (Figure 7b), indicating the beginning of the feedstock-gas mixing interface. At 200 s, the feedstock became well fluidized, as indicated by the yellow-to-red gradient for the feedstock, as shown in Figure 7c, with parallel behavior for nitrogen gas in Figure 7f. As the time step increases from 400 s to 800 s, as shown in Figures 8a to 8c for the feedstock, while the volume fraction of nitrogen in Figure 8d,e, the bed expansion increases to approximately twice the initial height. This result was supported by Makkawi and Mohamed [28], where the mixture of sand and feedstock also reached twice the initial bed height during pyrolysis.

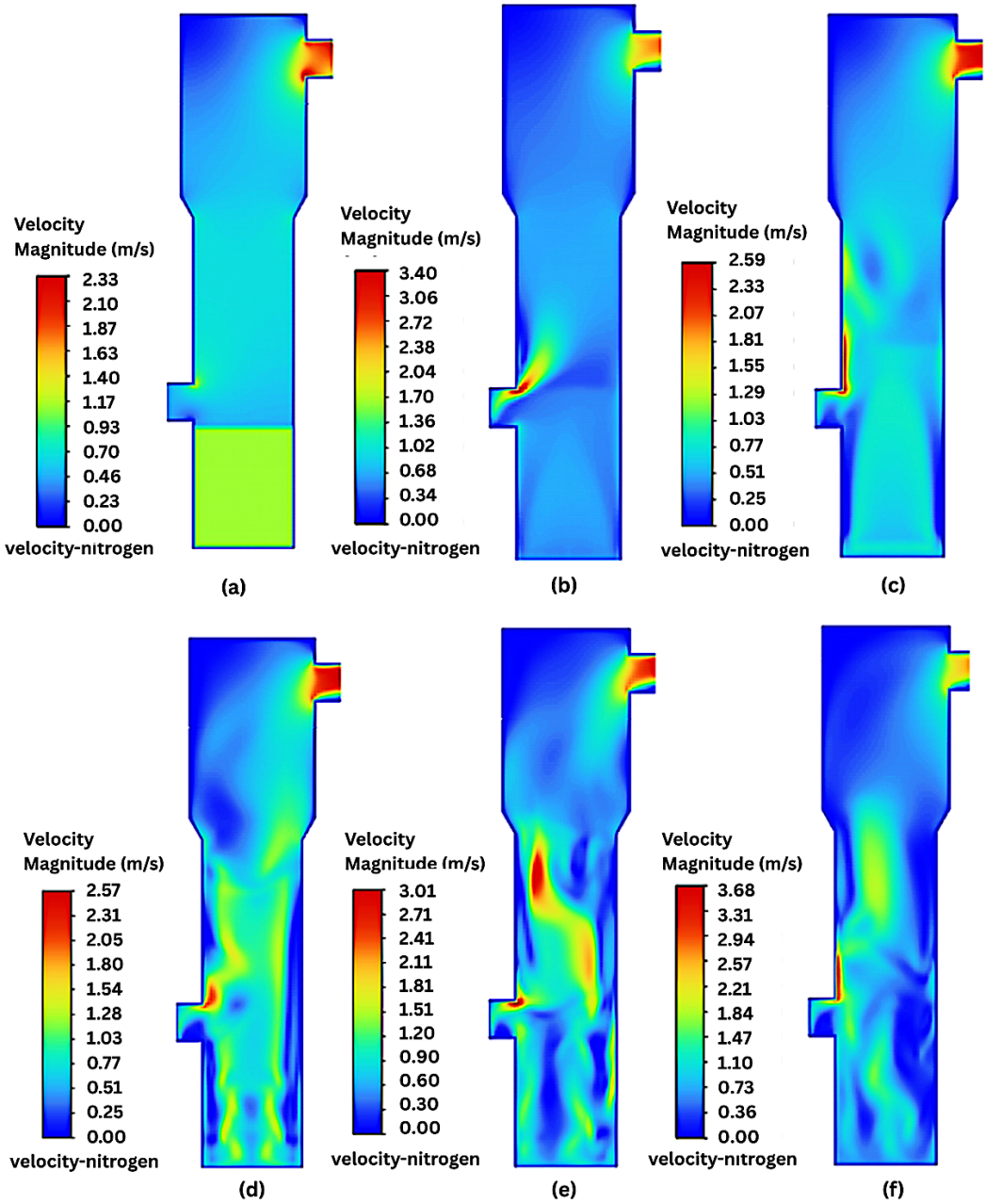

Figure 6. Time-average profile of the fluidizing nitrogen gas velocity during pyrolysis at (**a**) 0 s, (**b**) 100 s, (**c**) 200 s, (**d**) 400 s, (**e**) 600 s, (**f**) 800 s.

The formation of bubbles inside the vertical reactor is also observed. During pyrolysis, as the nitrogen gas was supplied at the bottom of the reactor, the solid feedstock was suspended and behaved like a fluid. As the gas flows inside the reactor, bubbles form due to the movement of particles and the expansion of the gas. This behavior was similar to that reported in other literature. Bubbles indicating good mixing were observed inside the reactor in the study of Makkawi and Mohamed [28], and Pourhoseinian, Asasian-Kolur and Sharifian [23]. It was also highlighted in the study of Luo et al. [34] for both feedstocks at 10 mm particle size undergoing pyrolysis at temperatures of 600 K and 800 K. Given the solid volume fraction of 60%, the time-averaged profile indicated that the reactor was continuously filled with nitrogen gas, as observed from the red-colored contour. This suggested a favorable condition with minimal to no oxidation process.

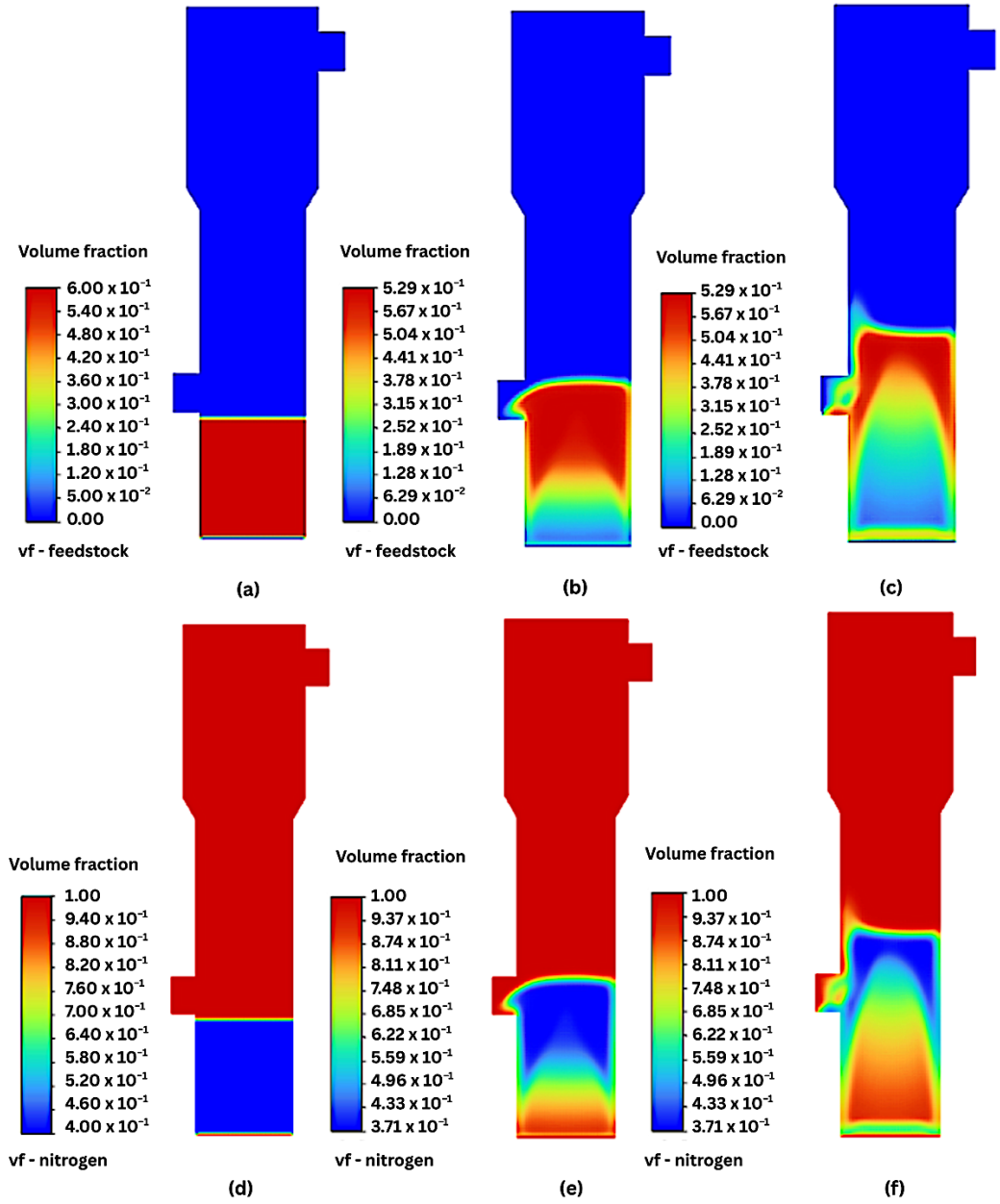

Figure 7. Contours of volume fraction distribution of solid-gaseous phase component: Solid biomass at (**a**) 0 s, (**b**) 100 s, (**c**) 200 s, nitrogen gas at (**d**) 0 s, (**e**) 100 s, (**f**) 200 s.

Another important aspect to investigate is whether the feedstock settles at the bottom of the reactor. At the start of the simulation, as shown in Figure 7d, nitrogen gas supplied from the bottom of the reactor pushes the solid feedstock upward. As the simulation progresses from 400 s to 800 s, the feedstock particles are mixed with the nitrogen gas (Figure 8a,c), indicating that the particles have been effectively suspended and dispersed throughout the flow. The simulation results reveal that the feedstock particles remain consistently suspended and mixed with nitrogen gas. This suggests that the nitrogen gas velocity was sufficient and that the particle size of the feedstock was appropriate for maintaining this level of mixing. The parallel behavior was also observed for the nitrogen gas in Figure 8d,f.

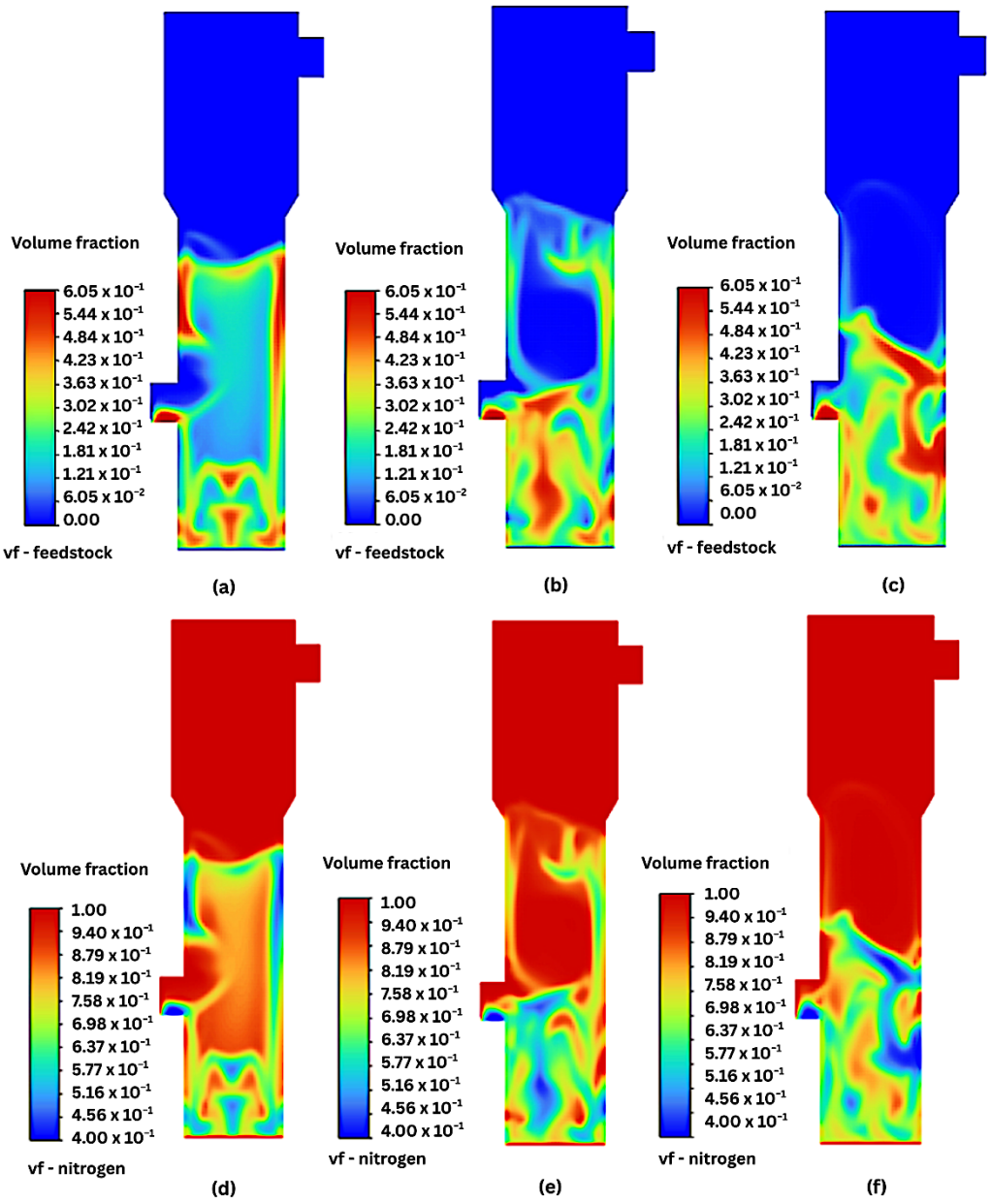

Figure 8. Contours of volume fraction distribution of solid-gaseous phase component: Solid biomass at (**a**) 400 s, (**b**) 600 s, (**c**) 800 s, nitrogen gas at (**a**) 400 s, (**b**) 600 s, (**c**) 800 s.

4. Conclusions

The fluid dynamics within a feedstock reactor for pyrolysis were successfully investigated using CFD with the Eulerian Multiphase Model. The simulation result provided insights into the behavior of nitrogen gas and biomass feedstock inside the vertical reactor during pyrolysis. The analysis includes the velocity profile, flow patterns of solid and gas phases, and mixing behavior. Convergence criteria and mesh independence were included to validate the accuracy of the computational model.

The study highlights the critical influence of operating conditions, feedstock size, and reactor geometry. The simulation, validated using a time-averaged profile, demonstrates that a 0.55 mm diameter feedstock particle with a bulk density of 536 kg/m^3 and a continuous nitrogen gas supply at 0.485 m/s exhibits a good mixing behavior. The feedstock velocity peaks at 0.98 m/s, resulting in significant bed expansion, which is twice the initial bed height. At a 25% loading capacity, equivalent to 9.5 cm from the reactor bottom, the bed expanded to 26 cm but remained below the gas outlet section. Additionally, the solid phase volume fraction decreases significantly from 0.6 to a range of 0.1 to 0.3, indicating continuous mixing that results in efficient temperature distribution and heat transfer.

Furthermore, the vertical reactor design facilitates efficient heat distribution, thereby reducing the risk of incomplete pyrolysis. While the optimized operating conditions were developed based on the specific scale and

configuration of the experimental reactor used in this study, they may not directly apply to reactors with different designs. However, the methodological framework, which integrates Eulerian multiphase modeling to assess flow dynamics, particle distribution, and mixing behavior, can be adapted and applied to other reactor configurations, offering a valuable approach for optimization across various pyrolysis systems.

The study highlights that feedstock particle size, loading capacity, inert gas velocity, and reactor design enhance pyrolysis efficiency. Key factors, such as bubble formation, bed expansion, and the interaction between the solid and gas phases, lead to a maximized yield and improved thermal performance. While vertical reactors offer superior phase separation, non-uniform temperature gradients require further investigation. CFD simulations can provide valuable insights into flow patterns and phase interactions through time-averaged profiles, enabling the assessment of the impact of multiple parameters on pyrolysis performance. Moreover, CFD is a powerful tool for scaling up pyrolysis processes by optimizing design, enhancing efficiency, and predicting performance at larger scales.

Recommendations include incorporating complex phenomena such as particle collisions, frictional interactions, and density variations during devolatilization to enhance the model's predictive accuracy. Furthermore, validating the simulation results through actual experimental studies is recommended to represent actual reactor conditions better and improve the reliability and applicability of the CFD model.

Author Contributions: D.R.R.C.: conceptualization, methodology, investigation, formal analysis, writing—original draft; A.T.U: conceptualization, formal analysis, writing—review and editing. All authors have read and agreed to the published version of the manuscript.

Funding: This research received no external funding.

Institutional Review Board Statement: Not applicable.

Informed Consent Statement: Not applicable.

Data Availability Statement: Data will be made available on request

Acknowledgments: The author extends gratitude to the Engineering Research and Development for Technology Department of Science and Technology (DOST-ERDT) for providing financial support to the first author.

Conflicts of Interest: The authors declare no conflict of interest.

Use of AI and AI-assisted Technologies: No AI tools were utilized for this paper.

Nomenclature

$\vec{g}$	gravity ($m \cdot s^{-2}$)
H	Enthalpy
K	solid-solid momentum exchange coefficient ($kg \cdot m^{-3} \cdot s^{-1}$)
k_{Θ_s}	Kinetic diffusion coefficient ($kg \cdot m^{-3} \cdot s^{-1}$))
k_s	The thermal conductivity coefficient ($W \cdot m^{-1} \cdot K$)
P	pressure (Pa)
Q_{gs_i}	Heat transfer coefficient ($W \cdot m^{-2} \cdot K^{-1}$)
S	Source ($kg \cdot m^{3} \cdot s^{-1}$)
t	Time (s)
T	Temperature (K)
V	Velocity vector ($m \cdot s^{-1}$)
∇	Divergence operator
∇p	Pressure gradient
β	momentum exchange coefficient ($kg \cdot m^{-3} \cdot s^{-1}$)
ρ	Density ($kg \cdot m^{-3}$)
α	phase volume fraction (-)
Θ_s	granular temperature ($m\ s^{-2}$)
$\acute{t}$	stress tensor (Pa)
γ_{Θ_s}	collisional dissipation of energy ($kg \cdot m^{-1} \cdot s^{-3}$)
φ_{ls}	energy exchange between the fluid and solid ($kg \cdot m^{-1} \cdot s^{-3}$)
Φ	angle of internal friction (-)
ζ_{nm}	Momentum exchange between solid phase *n* and other solid phases *m*
δ, γ	reaction equations stoichiometry coefficients (-)
g	Gas phase
s	solid phase
n, m	phase

References

1. IEA. CO_2 Emissions in 2023. Available online: https://www.iea.org/reports/co2-emissions-in-2023 (accessed on 8 August 2025).
2. Kurniawan, T.A.; Ali, S.; Mohyuddin, A.; et al. Cultivating sustainability: Harnessing biochar-derived composites for carbon-neutral wastewater treatment. *Process Saf. Environ. Prot.* **2024**, *187*, 665–697. https://doi.org/10.1016/j.psep.2024.04.040.
3. Hanson, E.; Nwakile, C.; Hammed, V.O. Carbon capture, utilization, and storage (CCUS) technologies: Evaluating the effectiveness of advanced CCUS solutions for reducing CO_2 emissions. *Results Surf. Interfaces* **2025**, *18*, 100381. https://doi.org/10.1016/j.rsurfi.2024.100381.
4. Biswal, B.K.; Balasubramanian, R. Use of biomass-derived biochar as a sustainable material for carbon sequestration in soil: Recent advancements and future perspectives. *NPJ Mater. Sustain.* **2025**, *3*, 26. https://doi.org/10.1038/s44296-025-00066-8.
5. Ubando, A.T.; Rivera, D.R.T.; Chen, W.-H.; et al. A comprehensive review of life cycle assessment (LCA) of microalgal and lignocellulosic bioenergy products from thermochemical processes. *Bioresour. Technol.* **2019**, *291*, 121837. https://doi.org/10.1016/j.biortech.2019.121837.
6. Rivera, D.R.T.; Culaba, A.B.; Ubando, A.T.; et al. The Environmental Performance of Torrefied Microalgae Biomass using Torrefaction Severity Factor. In Proceedings of the 2019 IEEE 11th International Conference on Humanoid, Nanotechnology, Information Technology, Communication and Control, Environment, and Management (HNICEM), Laoag, Philippines, 29 November 2019–1 December 2019; pp. 1–5.
7. Khodaei, H.; Álvarez-Bermúdez, C.; Chapela, S.; et al. Eulerian CFD simulation of biomass thermal conversion in an indirect slow pyrolysis rotary kiln unit to produce biochar from recycled waste wood. *Energy* **2024**, *288*, 129895. https://doi.org/10.1016/j.energy.2023.129895.
8. Escalante, J.; Chen, W.-H.; Tabatabaei, M.; et al. Pyrolysis of lignocellulosic, algal, plastic, and other biomass wastes for biofuel production and circular bioeconomy: A review of thermogravimetric analysis (TGA) approach. *Renew. Sustain. Energy Rev.* **2022**, *169*, 112914. https://doi.org/10.1016/j.rser.2022.112914.
9. Sangaré, D.; Moscosa-Santillan, M.; Bostyn, S.; et al. Multi-step kinetic mechanism coupled with CFD modeling of slow pyrolysis of biomass at different heating rates. *Chem. Eng. J.* **2024**, *479*, 147791. https://doi.org/10.1016/j.cej.2023.147791.
10. Lu, L.; Gao, X.; Dietiker, J.-F.; et al. MFiX based multi-scale CFD simulations of biomass fast pyrolysis: A review. *Chem. Eng. Sci.* **2022**, *248*, 117131. https://doi.org/10.1016/j.ces.2021.117131.
11. Guran, S. Chapter 8—Sustainable Waste-to-Energy Technologies: Gasification and Pyrolysis. In *Sustainable Food Waste-to-Energy Systems*; Trabold, T.A., Babbitt, C.W., Eds.; Academic Press: San Diego, CA, USA, 2018; pp. 141–158.
12. Zawawi, M.H.; Saleha, A.; Salwa, A.; et al. A review: Fundamentals of computational fluid dynamics (CFD). In Proceedings of the Green Design and Manufacture: Advanced and Emerging Applications: Proceedings of the 4th International Conference on Green Design and Manufacture, Ho Chi Minh, Vietnam, 29–30 April 2018; p. 020252.
13. Sumner, J.; Watters, C.S.; Masson, C. CFD in Wind Energy: The Virtual, Multiscale Wind Tunnel. *Energies* **2010**, *3*, 989–1013. https://doi.org/10.3390/en3050989.
14. Tian, W.; Han, X.; Zuo, W.; et al. Building energy simulation coupled with CFD for indoor environment: A critical review and recent applications. *Energy Build.* **2018**, *165*, 184–199. https://doi.org/10.1016/j.enbuild.2018.01.046.
15. Al-abidi, A.A.; Bin Mat, S.; Sopian, K.; et al. CFD applications for latent heat thermal energy storage: A review. *Renew. Sustain. Energy Rev.* **2013**, *20*, 353–363. https://doi.org/10.1016/j.rser.2012.11.079.
16. Mohamed, M.H.; Ali, A.M.; Hafiz, A.A. CFD analysis for H-rotor Darrieus turbine as a low speed wind energy converter. *Eng. Sci. Technol. Int. J.* **2015**, *18*, 1–13. https://doi.org/10.1016/j.jestch.2014.08.002.
17. Chen, J.; Xu, F.; Tan, D.; et al. A control method for agricultural greenhouses heating based on computational fluid dynamics and energy prediction model. *Appl. Energy* **2015**, *141*, 106–118. https://doi.org/10.1016/j.apenergy.2014.12.026.
18. Singh, R.I.; Brink, A.; Hupa, M. CFD modeling to study fluidized bed combustion and gasification. *Appl. Therm. Eng.* **2013**, *52*, 585–614. https://doi.org/10.1016/j.applthermaleng.2012.12.017.
19. Tobo, Y.; Lotfi, A.; Virla, L.D.; et al. Fast pyrolysis multiphase CFD-kinetics model in a drop tube reactor. *Fuel* **2023**, *340*, 127524. https://doi.org/10.1016/j.fuel.2023.127524.
20. Hartge, E.-U.; Ratschow, L.; Wischnewski, R.; et al. CFD-simulation of a circulating fluidized bed riser. *Particuology* **2009**, *7*, 283–296. https://doi.org/10.1016/j.partic.2009.04.005.
21. Kaczor, Z.; Buliński, Z.; Werle, S. Modelling approaches to waste biomass pyrolysis: A review. *Renew. Energy* **2020**, *159*, 427–443. https://doi.org/10.1016/j.renene.2020.05.110.
22. Janajreh, I.; Raza, S.S. Numerical simulation of waste tyres gasification. *Waste Manag. Res.* **2015**, *33*, 460–468. https://doi.org/10.1177/0734242X15573656.

23. Pourhoseinian, M.; Asasian-Kolur, N.; Sharifian, S. Comparative computational fluid dynamics analysis of fast pyrolysis of agricultural feedstocks across different biomass categories. *Biomass Bioenergy* **2024**, *180*, 107026. https://doi.org/10.1016/j.biombioe.2023.107026.
24. Wang, M.; Jia, T.; Song, X.; et al. CFD–DEM Simulation of Heat Transfer and Reaction Characteristics of Pyrolysis Process of MSW Heated by High-Temperature Flue Gas. *Processes* **2024**, *12*, 390. https://doi.org/10.3390/pr12020390.
25. Kamila, B.; Sadhukhan, A.K.; Gupta, P. 2D CFD modeling for pyrolysis of a large biomass particle: Effect of L/D ratio, internal convection and shrinkage. *Chem. Eng. Res. Des.* **2024**, *208*, 921–933. https://doi.org/10.1016/j.cherd.2024.07.002.
26. Wang, L.; Deng, J.; Yang, X.; et al. Role of biochar toward carbon neutrality. *Carbon Res.* **2023**, *2*, 2. https://doi.org/10.1007/s44246-023-00035-7.
27. Aniza, R.; Chen, W.-H.; Yang, F.-C.; et al. Integrating Taguchi method and artificial neural network for predicting and maximizing biofuel production via torrefaction and pyrolysis. *Bioresour. Technol.* **2022**, *343*, 126140. https://doi.org/10.1016/j.biortech.2021.126140.
28. Makkawi, Y.; Mohamed, B. CFD modeling of date palm (Phoenix dactylifera) waste fast pyrolysis in a fluidized bed-including experimental kinetics, validation, and remarks on the modeling approach. *Renew. Energy* **2024**, *224*, 120175. https://doi.org/10.1016/j.renene.2024.120175.
29. Gidaspow, D.; Bezburuah, R.; Ding, J. *Hydrodynamics of Circulating Fluidized Beds: Kinetic Theory Approach*; Illinois Institute of Technology: Chicago, IL, USA, 1991.
30. Lun, C.K.K.; Savage, S.B.; Jeffrey, D.J.; et al. Kinetic theories for granular flow: Inelastic particles in Couette flow and slightly inelastic particles in a general flowfield. *J. Fluid Mech.* **1984**, *140*, 223–256. https://doi.org/10.1017/S0022112084000586.
31. Syamlal, M. *The Particle-Particle Drag Term in a Multiparticle Model of Fluidization*; EG and G Washington Analytical Services Center, Inc.: Morgantown, WV, US, 1987.
32. Gunn, D.J. Transfer of heat or mass to particles in fixed and fluidised beds. *Int. J. Heat Mass Transf.* **1978**, *21*, 467–476. https://doi.org/10.1016/0017-9310(78)90080-7.
33. El may, Y.; Jeguirim, M.; Dorge, S.; et al. Study on the thermal behavior of different date palm residues: Characterization and devolatilization kinetics under inert and oxidative atmospheres. *Energy* **2012**, *44*, 702–709. https://doi.org/10.1016/j.energy.2012.05.022.
34. Luo, H.; Wang, X.; Liu, X.; et al. A review on CFD simulation of biomass pyrolysis in fluidized bed reactors with emphasis on particle-scale models. *J. Anal. Appl. Pyrolysis* **2022**, *162*, 105433. https://doi.org/10.1016/j.jaap.2022.105433.